



Numerical Study on the Effect of Bank Vegetation on the Hydrodynamics of the American River under Flood Conditions

Kevin Flora, P.E., D.WRE, M.ASCE¹; Christian Santoni, Ph.D.²; and Ali Khosronejad, Ph.D.³

Abstract: Vegetation can have an appreciable impact on the hydrodynamics and scour potential in natural rivers, but this effect is generally unaccounted for in high-fidelity computational fluid dynamic models. In this study, we have incorporated trees into the flow domain using two different approaches to study the hydrodynamics of the American River in Northern California under flood conditions. In the first approach, we resolved numerous trees as discrete objects. The second method incorporated a vegetation model into our in-house numerical model to treat the vegetation as a momentum sink along the banks. The flood flow of both cases was modeled using the large-eddy simulation. The computed hydrodynamics results of the cases were compared with a baseline case, which did not include any trees. Although both the tree-resolving and vegetation model approaches compared well with one another with respect to the flow field, they significantly altered the computed river flow dynamics and bed shear stress near the banks and the midwidth of the river compared with that of the no-tree case. Both methods that accounted for the resistance of the trees obtained lower and higher bed shear stresses and velocities along the banks and the midwidth of the river, respectively, than that of the baseline case. This research identified the important role that vegetation plays in natural rivers and provided researchers and engineers with the conceptual tools needed to incorporate vegetation into numerical models to improve the accuracy of the model results. DOI: 10.1061/(ASCE)HY.1943-7900.0001912. © 2021 American Society of Civil Engineers.

Introduction

In the application of real-world engineering problems, threedimensional (3D) numerical models have been used to study flow dynamics in riverine environments. Whereas unsteady Reynoldsaveraged Navier Stokes (URANS) turbulence models on relatively coarse grids have historically been the dominant numerical model for such studies, improved processing speeds available in highperformance computing (HPC) have also allowed for advanced turbulence modeling techniques, such as large eddy simulation (LES) to be used for various hydrodynamic studies, including those with natural rivers with submerged structures, such as piers (Khosronejad et al. 2012), rock vanes (Khosronejad and Flora 2018; Kang et al. 2016), and spur dikes (Jeon et al. 2018). LES efforts are indicated to obtain relatively more accurate and physics-based results for the flow dynamics of natural rivers, given their ability to resolve the large-scale and high-energy eddies in the river flow fields (Constantinescu 2014; Constantinescu et al. 2011; Koken and Constantinescu 2008; Koken et al. 2013). In other words, because the largest eddies possess the most energy, they are capable of

Note. This manuscript was submitted on September 24, 2020; approved on March 29, 2021; published online on June 29, 2021. Discussion period open until November 29, 2021; separate discussions must be submitted for individual papers. This paper is part of the *Journal of Hydraulic Engineering*, © ASCE, ISSN 0733-9429.

exerting the greatest influence on sediment transport and, thus, LES should provide more detailed and accurate flow characteristics about the instantaneous, turbulent flow field in natural rivers and the potential sediment transport processes, such as scour around bridge foundations and other hydraulic structures.

Despite the advanced turbulence modeling capabilities, natural river flows are highly complex with a wide range of turbulent eddy sizes, making it impossible to fully capture the intricate features using a numerical model. One common feature that is often neglected in high-fidelity modeling of natural rivers is the impact of vegetation on the flow and sediment dynamics. In fact, along with the channel geometry and boundary roughness, vegetationwhich obstructs the flow-is a dominant feature of flow in natural waterways that can have the strongest influence the flow distribution, flood inundation, and magnitude and location of sediment transport processes (Liu and Nepf 2016). The importance of vegetation impacts on the flow is well established and documented in past studies in which researchers have attempted to understand the interaction between turbulent flows and arrays of emergent and submerged stems (Liu et al. 2008; Poggi et al. 2004; Garcia et al. 2004; Ghisalberti and Nepf 2002; Wilson et al. 2003; Nepf 1999). Most numerical studies for flow through vegetation have been used in idealized flow environments with Reynolds-averaged Navier (RANS) turbulence models (Shimizu and Tsujimoto 1993; Lopez and Garcia 1996; Fischer-Antze et al. 2001; Choi and Kang 2004; Jahra et al. 2011). However, Stoesser et al. (2010) performed LES to simulate idealized structures of varying diameters and densities and found that the density of the structures was dominant in affecting the turbulence statistics and flow resistance.

Although most numerical studies have attempted to model vegetation using rigid or flexible geometric shapes such as cylinders, Shaw and Schumann (1992) simulated airflow through a series of trees using an LES model and a numerical canopy algorithm that extracts momentum from the airflow in the region of trees, thereby

¹Ph.D. Candidate, Civil Engineering Dept., College of Engineering and Applied Sciences, Stony Brook Univ., Stony Brook, NY 11794. ORCID: https://orcid.org/0000-0002-4476-0082

²Postdoctoral Associate, Civil Engineering Dept., College of Engineering and Applied Sciences, Stony Brook Univ., Stony Brook, NY 11794. ORCID: https://orcid.org/0000-0002-7578-2161

³Assistant Professor, Civil Engineering Dept., College of Engineering and Applied Sciences, Stony Brook Univ., Stony Brook, NY 11794 (corresponding author). ORCID: https://orcid.org/0000-0002-9549-3746. Email: ali.khosronejad@stonybrook.edu

providing a simplified means for incorporating the effects of trees into numerical models. The LES-computed aerodynamic/thermodynamic effects imposed by the plants compared favorably with field and wind tunnel measurements (Patton 1997). Yokojima et al. (2013, 2015) evaluated the effect of vegetation configuration on turbulent flows using LES and compared results using experimental data and emergent circular cylinders. They found that the LES results are in good agreement with the experimental results when the cylinders are continuous in the streamwise direction; however, the LES could not reproduce the experimental results for the case in which the cylinders were in patches. Yokojima et al. (2013, 2015) concluded that the problem with the canopy model is related to the uniform drag coefficient (C_d) value applied throughout the vegetation patches.

This study investigates the effects of vegetation on the hydrodynamic processes and the sediment transport potential in natural rivers using two different modeling methods. In one approach, we simulate 1,900 individual tree-like structures representative of typical trees along riverbanks by resolving their detailed geometry using the immersed boundary method (Khosronejad and Flora 2018, 2019; Khosronejad et al. 2019a, b, 2020a, b, c, d, e). In the second method, a vegetation model was developed to account for the effects of plants and trees on the turbulent flood flow of a natural river. To conduct these simulations, we employ the LES model of our in-house code, the so-called Virtual Flow Simulator (VFS-Geophysics) model (Calderer et al. 2015). The vegetation model adopted in this study uses a depth-varying drag coefficient that represents the effect of the tree trunks, branches, and leaves at different elevations. This approach improves on previous methods that have been used in numerical simulations for flumes by being more physically realistic with respect to the varying degrees of obstruction caused by trees in a natural river. LES results for both methods were compared against a baseline case, which neglects the vegetation altogether. We explore the influence of each technique using a case study at a reach of the American River in Northern California. This river's reach is 1,150-m long, approximately 140-m wide, and approximately 12.2-m deep. The study area contains four bridges, each having several bridge piers obstructing the flow, creating high levels of turbulence and modification to the hydrodynamics. In addition, the American River provides dense vegetation along each bank.

This paper is organized as follows. First, the hydrodynamic model and governing equations are introduced. Next, the site conditions of the case study site at the American River are described, followed by computational details for the numerical model. Subsequently, the results are presented along with pertinent discussions for how each of the two modeling approaches compared with the base model. Finally, the principal contribution of this study is highlighted, indicating the important role of vegetation on influencing the hydrodynamic and morphodynamic processes in natural rivers.

Governing Equations and Numerical Methods

The hydrodynamic model numerically solves the conservation of mass and Navier-Stokes equations for an incompressible flow, as follows (Khosronejad and Sotiropoulos 2014, 2017):

$$\frac{\partial u_j}{\partial x_j} = 0 \tag{1}$$

$$\frac{\partial u_i}{\partial t} + u_j \frac{\partial u_{i,}}{\partial x_i} = -\frac{1}{\rho} \frac{\partial P}{\partial x_i} + \nu \nabla^2 u_i + g_i \delta_{i3} + \frac{\partial \tau_{ij}}{\partial x_j} + F_i \qquad (2)$$

where u_i = velocity vector of the flow along the *i*-direction; ρ = density of water; P = pressure; ν = kinematic viscosity of water; g = gravitational body force; δ = Kronecker delta function; and F_i = body force per unit volume given by the vegetation model. The subgrid stresses, τ_{ij} , are modeled using the dynamic Smagorinsky eddy viscosity model (Smagorinsky 1963; Germano et al. 1991).

For the vegetation model, a drag force is macroscopically applied to the flow in regions delineated as those containing trees, thereby reducing the momentum of the flow. The drag force term, F_i , is defined as (Shaw and Schumann 1992)

$$F_i = -\rho C_d A_f(u_i u_i)^{1/2} u_i \delta(x_k - X_k) \tag{3}$$

where ρ = density of the water; C_d = drag coefficient; and A_f = projected area of the vegetation per unit volume. The Dirac delta, δ , distinguishes the grid points x_k for which the force is to be applied that is inside the vegetated region, X_k , from those outside of the vegetated area. The projected area in a vegetation model is determined using a predefined vertical distribution for the leaf area density known as the "frontal area density," which can vary for specific cases due to various factors, such as the tree species, plant density, and season of the year. The "frontal area density" function of the canopy varies with the height above ground, is defined with respect to its degree of blockage for the flow, and is determined as the cross-sectional frontal area blockage of the trees per unit volume. Examples of leaf area density distributions for deciduous trees with a relatively open trunk space can be found in Shaw and Schumann (1992). One such frontal area density distribution is illustrated in Fig. 1(b). Although Yokojima et al. (2013) argued that the canopy model results were not sensitive to the choice of drag coefficient, C_d , Morinaga et al. (2012) estimated the C_d for trees in flowing water to vary between 0.4 and 1.2. Their study considered the trunk roughness, sheltering effects, spacing, and inclination caused by bending trees. Sonnenwald et al. (2019) analyzed the drag caused by emergent vegetation and developed a relationship between diameter and solid volume fraction. They found that for high Reynolds numbers and low solid volume fractions, C_d was approximately 1.0. Three values of C_d , ranging from 0.3 to 1.0, are compared in this study.

The Virtual Flow Simulator (VFS)-Geophysics model is implemented using the curvilinear immersed boundary (CURVIB) method and can resolve arbitrarily complex geometric configurations, such as the channel bed and bridge piers. The CURVIB provides an excellent framework for handling the irregular, meandering shapes of natural rivers by providing an efficient mechanism for using orthogonal mesh elements for the fluid domain. An important capability of the VFS-Geophysics code for this study is its use of the immersed boundary method (IBM) for resolving complex objects, such as the bank line trees in natural rivers. IBM is a much simpler alternative numerical approach to using body-fitted meshes for incorporating geometric boundaries and objects into the flow domain (Gilmanov et al. 2003). With the IBM, a structural body mesh comprised of a solid object(s) is superposed on the background Eulerian fluid mesh that is kept fixed. With the IBM, each of the domain nodes is categorized as being a fluid node, a solid node, or an immersed boundary (IB) node depending on its location with respect to the position of the body (Gilmanov and Acharya 2008; Khosronejad et al. 2011). The nodes that fall inside the IB body are considered solid nodes and are removed from the computational domain. The nodes that are in the fluid but adjacent to the solid boundaries are identified as IB nodes. The IB nodes are the location at which the boundary condition of the velocity field is reconstructed. Natural riverine flows have a high Reynolds number, making it practically impossible to resolve the viscous sublayer

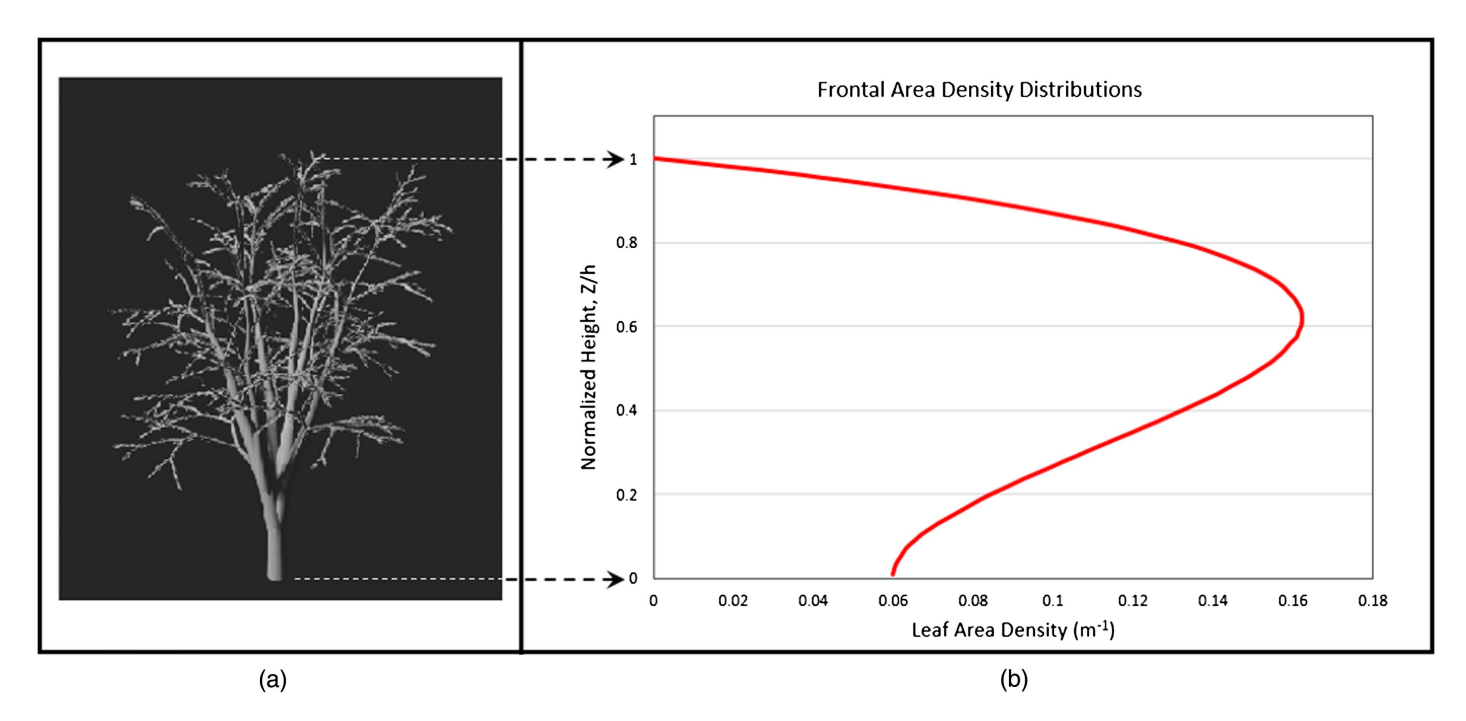


Fig. 1. Frontal area density distributions used in vegetation model indicating: (a) a generalized tree shape; and (b) corresponding variation in frontal area density (A_f) normalized by tree height (h).

near the solid surfaces. Instead, the IB node velocity reconstruction uses a wall model at the solid boundaries that is explained in detail in Khosronejad and Sotiropoulos (2014). The remaining nodes are the fluid nodes at which the governing equations are solved. Fig. 2 illustrates how the IBM algorithm in our in-house code classifies the computational nodes of the background mesh to solid, IB, and fluid nodes when objects such as a tree trunk or channel bed are immersed in the flow domain.

The governing equations are discretized on a hybrid staggered/ nonstaggered grid arrangement (Gilmanov and Sotiropoulos 2005; Ge and Sotiropoulos 2007). Spatially, the accuracy of the discretization is second-order for the convective, divergence, pressure gradient, and viscous terms. Similarly, the temporal derivatives use a second-order backward differencing discretization scheme. The pressure and momentum equations are solved using the second-order accurate fractional step method in which the momentum equation is

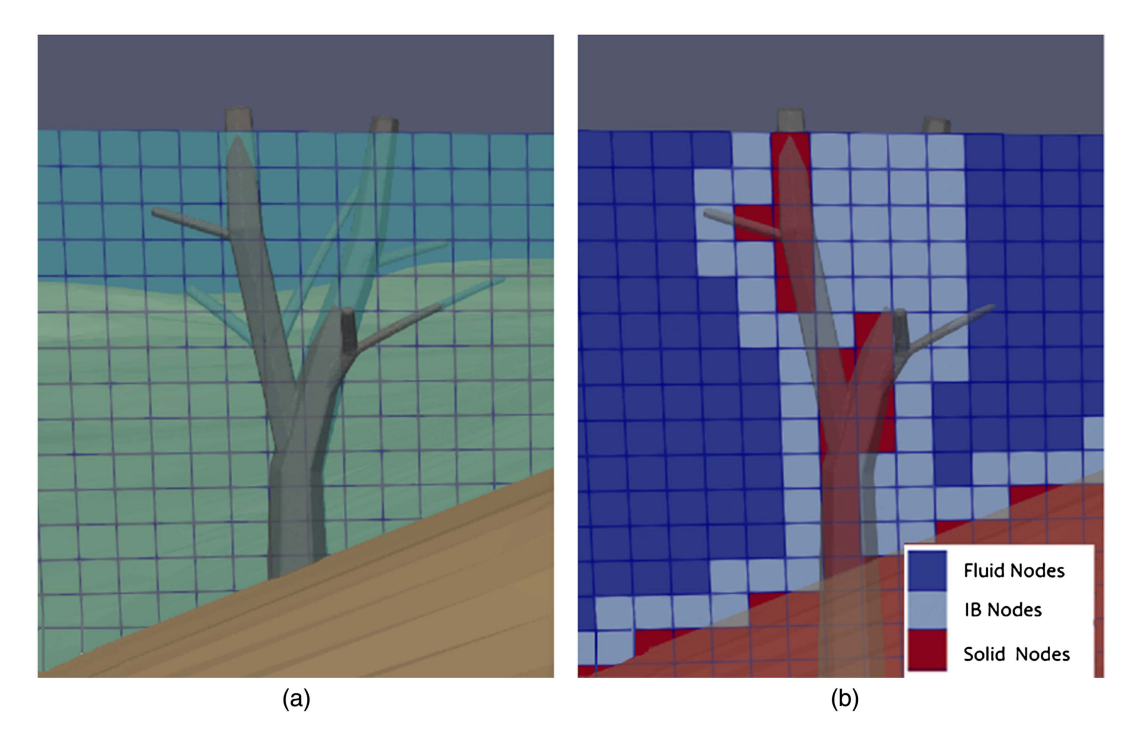


Fig. 2. (a) Schematic of tree trunk placed on flood plain of river in background mesh; and (b) classification of background mesh into fluid, solid, and IB nodes, respectively.

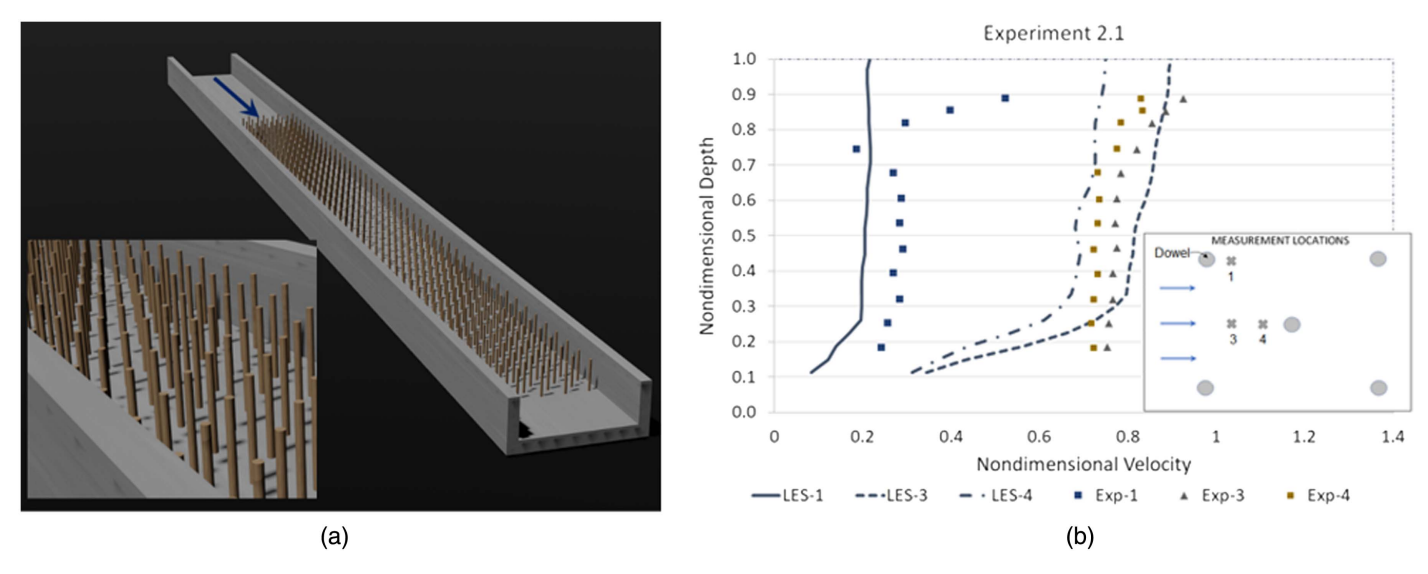


Fig. 3. Numerical model validation results for test case reported by Liu et al. (2008) involving open channel flow in laboratory flume with wall-mounted cylinders as indicated in (a). (b) Streamwise velocity profile at three different locations compared relative to experimental measurements. (Data from Liu et al. 2008.)

solved using a Jacobian-free, Newton-Krylov solver for the momentum equations. The Poisson equation is solved using a generalized minimal residual method (GMRES) solver coupled with an algebraic multigrid preconditioner.

Validation Study

The VFS-Geophysics model has been extensively validated for flow computations of experiments in laboratory flumes and field measurements in full-scale channels and natural rivers. For instance, the code has been validated for measured field velocity data on the Mississippi River for base flow conditions (Le et al. 2019). In addition, the model was validated for bankfull flows of a field-scale channel at the Outdoor StreamLab of the St. Anthony Falls Laboratory at the University of Minnesota by Kang et al. (2011) and Khosronejad and Sotiropoulos (2014). For this study, validation of flow around cylindrical obstacles was performed by simulating the laboratory flume experiments of Liu et al. (2008) to assess the capability of the numerical code to model the flow around patches of obstacles (e.g., bank line trees). Specifically, this validation case compared Liu's measured data of the flow field around a staggered configuration of emergent, rigid dowels using the LES module of the VFS-Geophysics model. In Fig. 3(a), sample velocity data were collected in the center of the flume near the downstream end of the dowels and was nondimensionalized with a bulk velocity of 0.225 m/s and a mean flow depth of 0.065 m in the test case. As indicated in Fig. 3(b), the LES captured the first-order statistics of the flow in the water column. Some deviation from the measured results might reflect incomplete capturing of the small diameter dowels or uncertainty in the measured data. In the future, to improve our validation of the LES, we plan to collect velocity data in a natural river during a flood event that inundates bank vegetation.

Test Case Description and Computational Details

Study Area and Field Measurements

A case study of a natural river is used to test the impact of two alternative modeling techniques for incorporating bank line trees into a high-fidelity numerical model. Fig. 4 presents an aerial view of the case study site indicating a long reach of the American River located within the city of Sacramento, California. This site encompasses four bridges and is lined with mature trees, such as oak and willow, along the majority of both banks and provides an excellent opportunity to examine the effect that vegetation has on the flow dynamics in a natural river.

The American River is a major river in Northern California flowing out of the Sierra mountains, which passes through Sacramento, CA. Approximately 3.2 km downstream from the study site, the American River joins at the confluence with the Sacramento River. The study site is approximately 1,150 m in length, with an average width of 140 m encompassing the main channel of the river. The flow depth during a 100-year flood event ranges from 9.1 to 16.7 m due to the natural variation in the bathymetry with a mean-flow depth of ~12.2 m. The banks of the river are nearly fully lined with vegetation consisting primarily of mature oaks and willow trees. We developed the topography of the river by conducting a field campaign using a single beam survey onboard a boat to measure the river bathymetry in combination with aerial LiDAR data for the banks (Fig. S1).

In this study, we used a sloped rigid lid assumption to prescribe the water surface of the river, which has been indicated to be accurate enough for such applications (Khosronejad et al. 2019a). To confirm this conclusion, an assessment of the variation in the free surface was made using the level-set method, which indicated that the maximum deviation in the water surface was less than 10% of the flow depth throughout the entire reach of the river, indicating that the rigid lid assumption would not introduce significant errors in the simulation. The geometry and height of the rigid lid were determined in advance using a simplified two-dimensional model. A no-slip boundary was prescribed at the channel boundary and any solid objects (i.e., trees and bridge piers).

At the inlet, a precursor short, straight reach with uniform channel geometry equivalent in cross-sectional area to the inlet cross-section of the study reach was generated for the flow domain. A steady inflow discharge equivalent to 3,330 m³/s representing the design flow rate within the main channel was prescribed for the precursor case using periodic boundary conditions at the inlet and outlet. Once the flow in this precursor simulation reached a fully developed, turbulent flow state, the time-varying velocities



Fig. 4. Satellite image of American River site. (Map data © 2018 Google.)

at the outlet were stored for later use in the case study to provide a turbulent inlet profile. For model comparison purposes, the time series for the computed velocity and pressure were saved near the bed, mid-depth, and free surface at 15 locations in the river, as indicated in Fig. 5.

Computational Grid System

Three structured grids were generated with a uniform resolution of 1.20, 0.60, and 0.40 m, which corresponds to 3.1, 24.3, and 82.2 M

grid nodes for a coarse, medium, and fine grid, respectively. The wall distances, which were the same in all directions, were more than 1,000 for the coarse, medium, and fine grid systems, which made inevitable the use of the wall function at all solid boundaries. Additional details of the computational grid are provided in Table 1. Fig. S2 presents the time-averaged velocity magnitudes near the surface for each grid resolution. A comparison of the computed flow fields of the three grid systems reveals that the level of detail in the velocity distribution increases with the grid resolution; however, the general flow distribution and magnitude indicate only



Fig. 5. American River indicating: (a) study area limits; (b) overview; and (c) zoomed-in area where computed velocity components and pressure were saved. The mean-flow depth at the site is ~12.2 m. [Map data for (a) from Google Earth, Earth data © 2019 Google, Image Landsat/ Copernicus; map data for (b and c) from © Mapbox © OpenStreetMap © Maxar.]

minor differences between the medium [Fig. S2(b)] and fine [Fig. S2(c)] resolution cases. With respect to the turbulent kinetic energy (TKE) in the flow, contours of the TKE normalized with the bulk velocity are indicated on the log scale for each grid resolution

Table 1. Computational grid systems and time step employed for flow simulations

Variable	Coarse grid	Medium grid	Fine grid
$\overline{N_x \times N_y \times N_z}$	961 × 161 × 21	$1,921 \times 317 \times 41$	$2,881 \times 477 \times 61$
Δx , Δy , Δz (m)	1.22	0.60	0.40
x_{+}, y_{+}, z_{+}	90,000	45,000	22,500
Δt (s)	0.22	0.05	0.05
Number of	3.25×10^{6}	25.0×10^{6}	83.8×10^{6}
grid nodes			

Note: x, y, and z represent the streamwise, spanwise, and vertical directions. Nx, Ny, and Nz are the number of grid nodes and the grid spacing of the background grid for the flow solver in each direction. x^+ , y^+ , and z^+ are the nondimensional wall distances. Δt is the temporal step of the simulation.

at the free surface in Fig. S3. Comparing grid resolutions, the TKE increases with grid resolution, as observed downstream from the piers and in many locations along the channel banks.

Comparing the specific time histories for a selected point sampled in the channel can demonstrate how the degree of fluctuation in the flow velocity and how well each case captures the energetic structures in the flow. A point (i.e., point #14 in Fig. 5) located downstream of the last bridge in the flow in the center of the channel was selected for this purpose. The power spectral density of each grid resolution [Fig. S4(b)] indicates that each grid captured the energy production range (0.02–0.08 Hz) and inertial subrange (0.08–0.2 Hz). The amount of fluctuation in the velocity magnitude for all resolutions varied by approximately 15% from the mean velocity magnitude.

In summary, the essential features of the main channel flow are captured well by all three grid resolutions. The fine resolution grid provides the most detailed depiction of the flow characteristics; however, the high computational cost required to perform LES makes using this resolution prohibitive. As a result, the medium

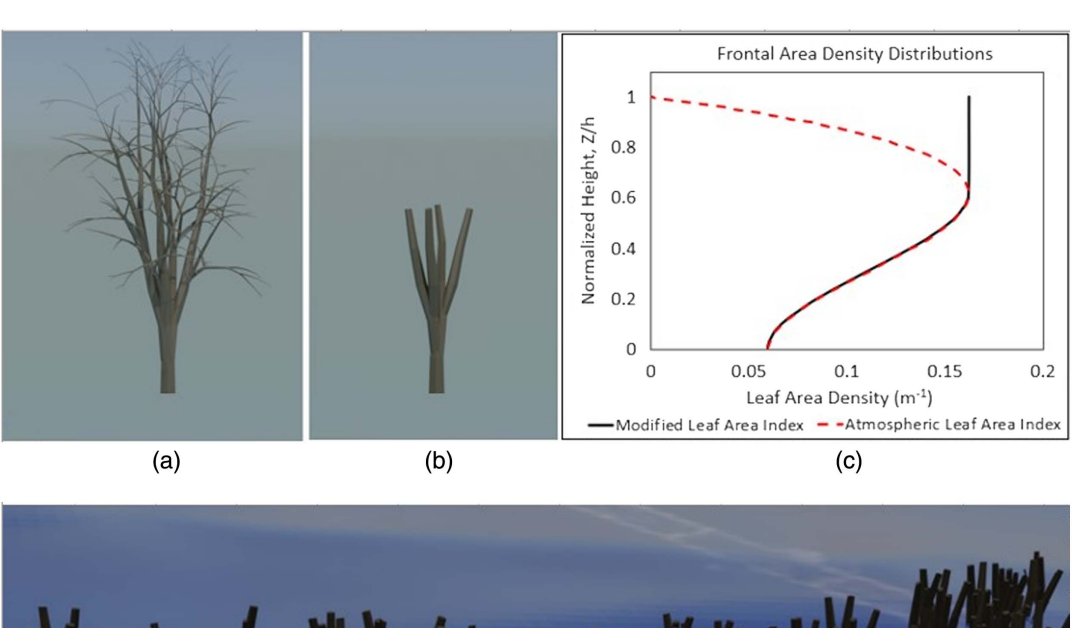




Fig. 6. Computer-generated tree shapes indicating (a) tree with full canopy; (b) truncated tree resolved in numerical model; (c) modification to frontal density area in vegetation model to account for upper portions of trees not being submerged in the flow—dashed line reflects a typical distribution in atmospheric flows for which entire tree height contributes to blocking the flow; solid line represents the submergence of only trunk and upper limbs in water flow of water; and (d) example of inundated trees.

resolution grid provides a reasonable compromise with respect to computational demands and hydrodynamic details and is used for the LES of the vegetation approaches.

Generation of Discrete Trees for Tree Resolving Model

To simulate flow through a tree-lined bank, more than 1,900 discrete trees were created using the free and open-source 3D computer graphics software, Blender. Full-scale, realistic-shaped trees were easily generated in Blender using the *Sapling Tree Generator* plugin, which allows one to create simplified models of trees by selecting the species, size, shape, and branch geometries for the test case that are similar to the willows and oaks found along the American River. However, for simplification of the numerical modeling, the upper portions of the modeled trees, including the leaves, twigs, and small branches, were truncated, leaving only the trunks and lower major limbs to be submerged in the water during the simulation, as depicted in Fig. 6(b).

The tree trunks were placed with Blender using the *Scatter Objects* plugin, which allows one to control the density, scale, and randomness of the size and orientation of the trunks because they were placed in the general location and with the approximate density, as observed for the actual trees in satellite imagery [Fig. 7(a)]. The random variation in the size and orientation feature was applied to the trunks to create a more natural environment. Typically, the diameter of the tree trunks varied between 0.6 and 0.8 m. Each of these individual trunks was exported as individual unstructured triangulated surfaces and used as an immersed object in VFS-Geophysics. During the simulation, the trunks were submerged to varying degrees in the flow based on their location on the bank and the individual tree height [Fig. 6(d)].

Vegetation Model Delineation and Parameterization

Using a similar approach to that of the tree-resolving placement, the vegetation model required distinct regions to be delineated according to their spatial location in the real world. Satellite imagery was used as a background, and Blender was used to draw eight separate areas that were then extruded to create canopy volumes [Fig. 7(b)].

Because the vegetation model is adapted from the canopy model used in atmospheric flows for riverine environments, it is necessary to adjust the frontal area density curve to account for the typical riverine case in which the upper portion of the tree canopy is not typically submerged in the water. To do this, it is assumed that there is no reduction in the leaf density at the maximum height of the tree, which is submerged in the water. In other words, near the water surface, it is likely that the maximum leaf density might be exposed to the flow throughout the upper region of the flow, as indicated by the vertical line in the modified curve in Fig. 6(c). The drag coefficient, C_d , of the vegetated area (representing trees) was set at 0.74, which is within the range estimated by other researchers for flow through emergent vegetation (Morinaga et al. 2012; Sonnenwald et al. 2019). As with the case using the resolved trees, the vegetation model is intended to apply a varying drag force to the flow based on the height above the ground.

Results and Discussion

This section presents the computed flow field within the case study area using three cases: (1) no vegetation, (2) tree-resolving model, and (3) vegetation model. It is anticipated that including vegetation in the computations will redistribute the flow and modify the turbulence in the flood flow within the river. Both effects are important for understanding and predicting erosion and scour processes at the base of the bridge foundations and the riverbanks. In addition, these effects are also relevant for fish habitat and channel restoration studies (Peters et al. 1996; Carollo et al. 2002; Thorne 1990).

In Figs. 8 and 9, we plot contours of the LES computed instantaneous velocity magnitude (nondimensionalized with the meanflow velocity, U = 2.24 m/s) and the time- and depth-averaged

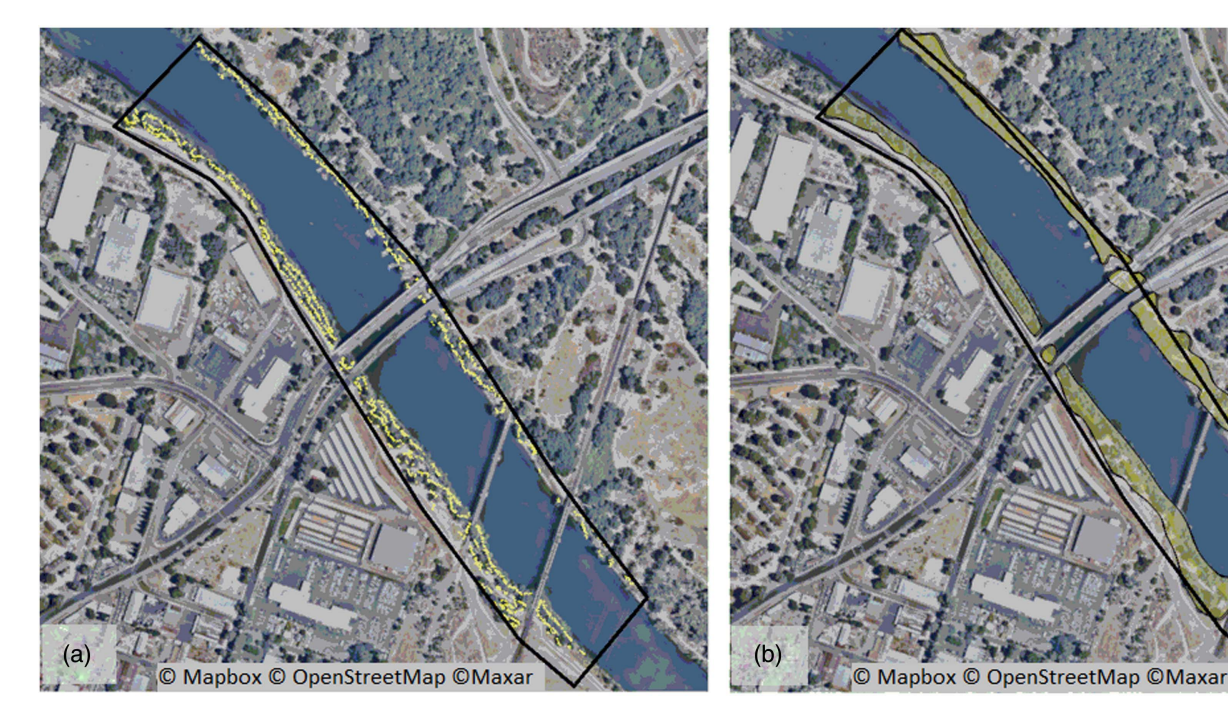


Fig. 7. Locations of (a) individual trees; and (b) vegetated regions highlighted within study area (solid line). (Base map © Mapbox © OpenStreetMap © Maxar.)

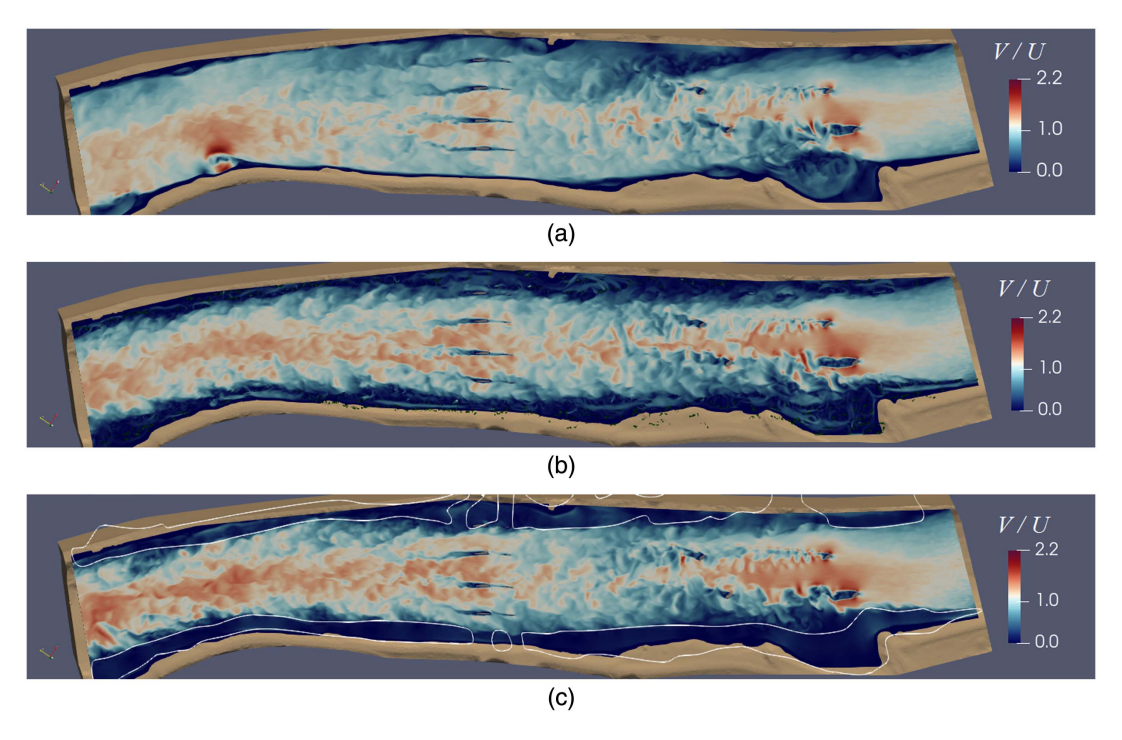


Fig. 8. Contours of instantaneous velocity magnitude (V) at water surface normalized with mean-flow velocity (U = 2.24 m/s) for cases (a) without trees; (b) resolved trees; and (c) vegetation model in which the outline near banks represents vegetated regions. The mean-flow depth is 12.2 m and is conveyed from right to left.

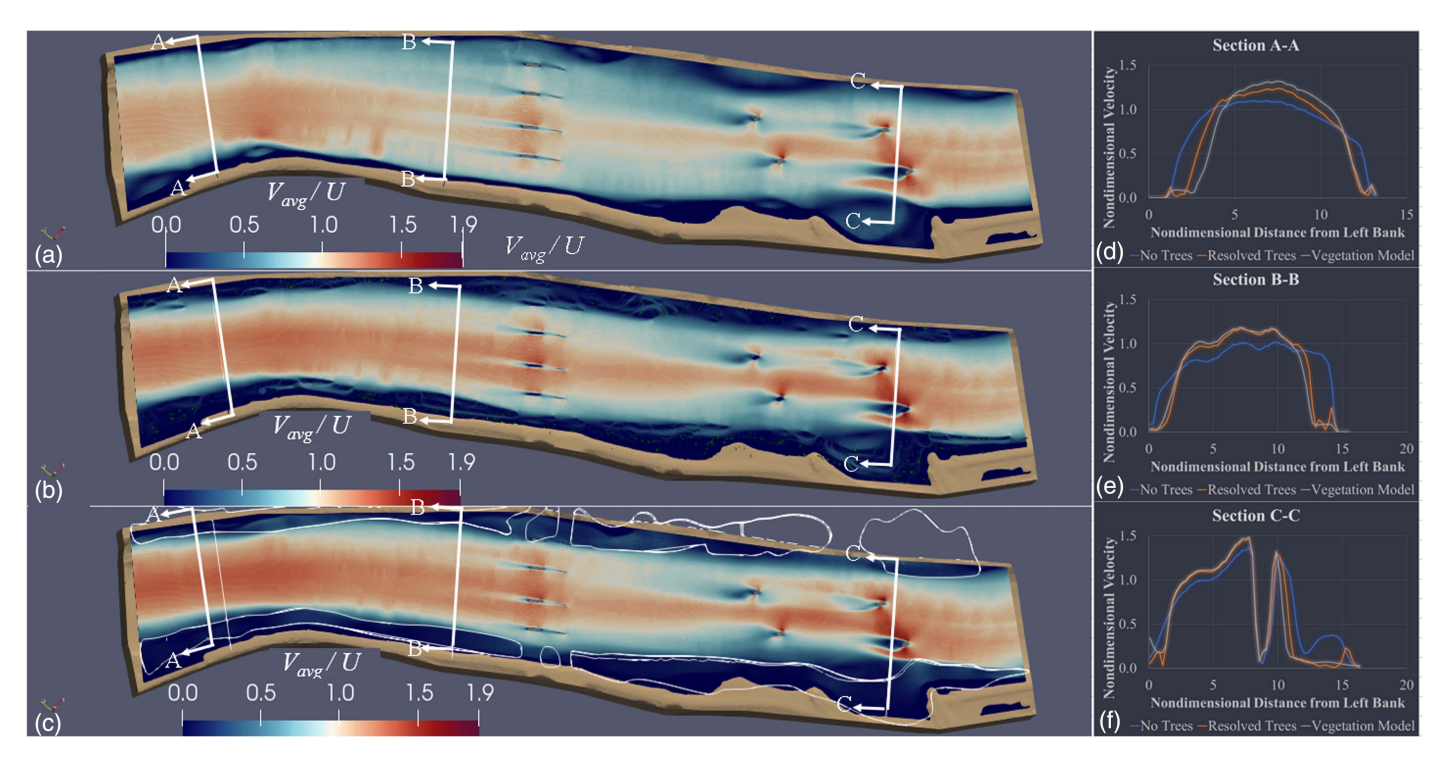


Fig. 9. Contours of time- and depth-averaged velocity magnitude (V_{avg}) normalized with mean-flow velocity (U = 2.24 m/s) for cases (a) without trees; (b) resolved trees; and (c) vegetation model with vegetated regions are outlined near the banks. The three lines across the river in each figure are cross-section locations indicating how the velocity magnitude compares for each case in which Sections A-A, B-B, and C-C are indicated in (d-f). Horizontal distance is normalized by mean-flow depth of \sim 12.2 m, and flow is conveyed from right to left.

velocity magnitude for each simulation. As observed, both types of vegetation approaches (tree-resolving and vegetation model) have a significant impact on the computed flow field by diverting the high-velocity core of the flood away from the banks toward the center of

the channel. For the case without vegetation [Figs. 12(a) and 13(a)], the flow is distributed throughout the full river width, with high velocities near the banks. In contrast, both cases that incorporated vegetation have much wider regions at each bank with

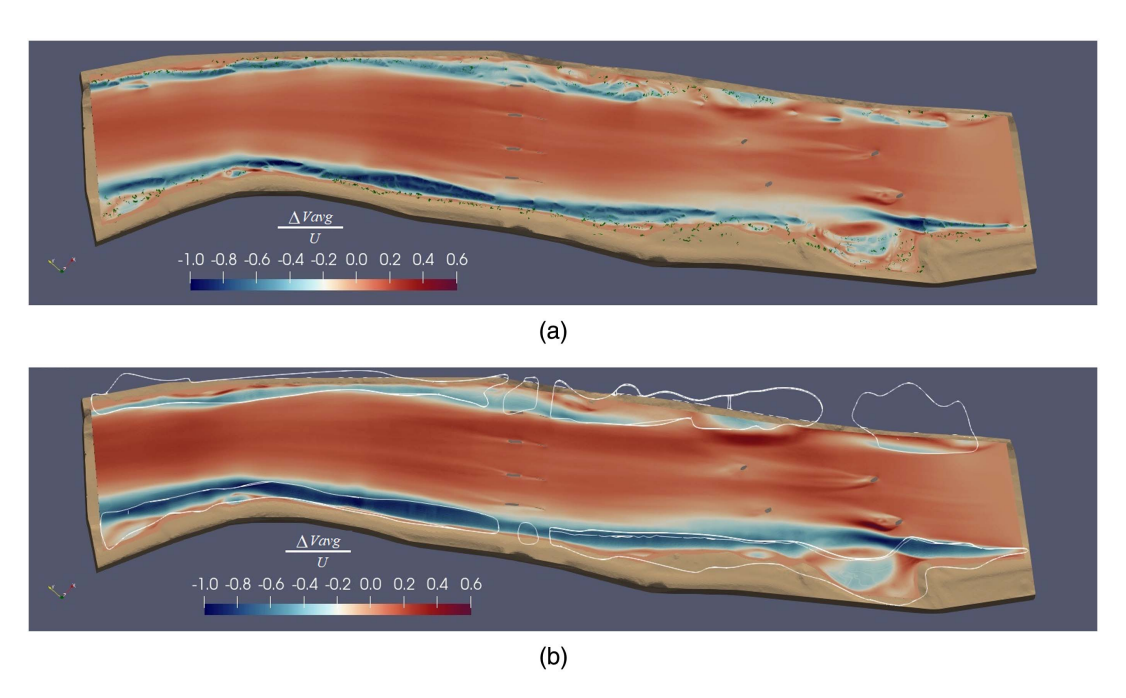


Fig. 10. Contours of time- and depth-averaged velocity magnitude difference between vegetated simulations and base case without vegetation for (a) tree resolving case; and (b) vegetation model. The mean-flow depth is ~12.2 m and is conveyed from right to left.

slow velocities. Consequently, both approaches also have increased velocities near the center of the channel. To highlight the effect on the flow distribution, Fig. 10 indicates the difference in the normalized velocity magnitude ($\Delta V/U$) for each vegetated case by subtracting the no vegetation case depth–averaged velocity magnitude from each of the vegetated cases. The results indicate that the normalized depth-averaged velocity along both banks is reduced by approximately 1, and the normalized depth-averaged velocity in the

center of the channel increases by approximately 0.6. The change in the velocity distribution caused by the vegetation is noticed not only at the surface but also impacts the flow throughout the entire depth. Fig. 11 indicates how the time-averaged velocity is redistributed throughout the flow depth. This effect is particularly noticeable near the left bank, where both vegetated models indicate significant decreases in velocity. In addition, this influence is observed to laterally reduce the flow velocity well into the main channel.

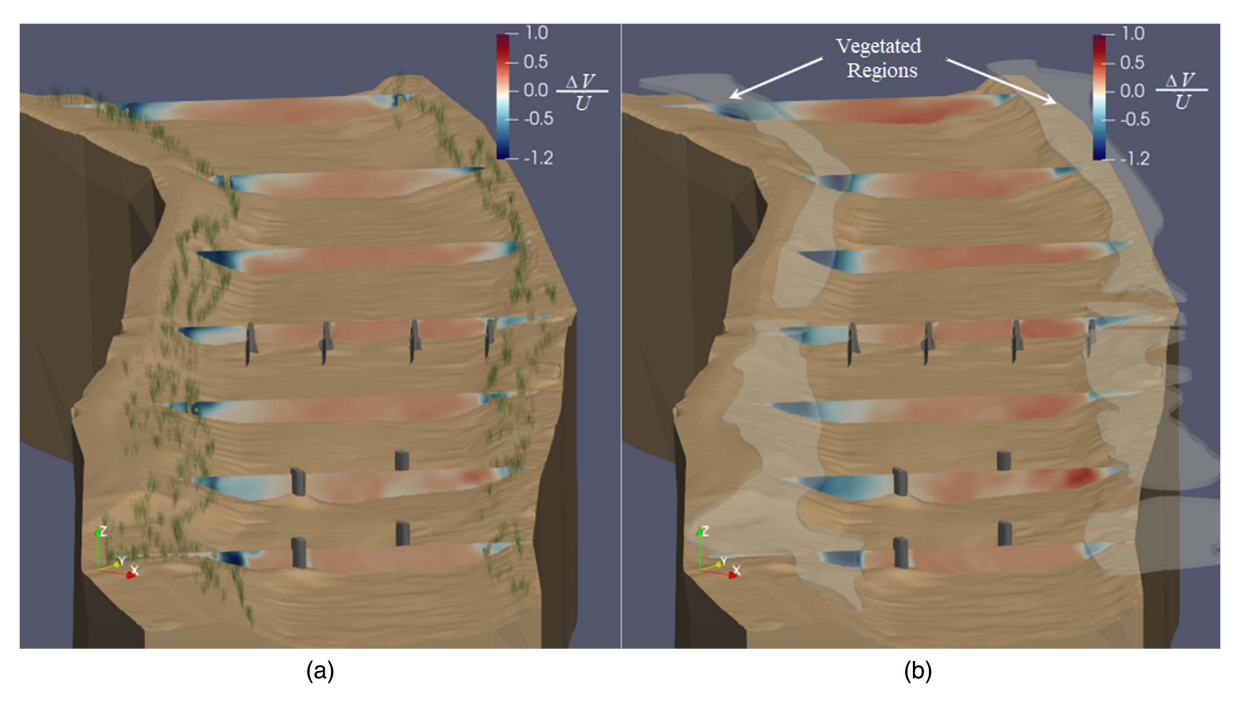


Fig. 11. Contours of time-averaged velocity magnitude difference between two vegetated simulations and simulation without vegetation at several channel cross-sections along the river for: (a) tree resolving case; and (b) vegetation model. Translucent regions represent vegetated areas. Flow is from bottom to top.

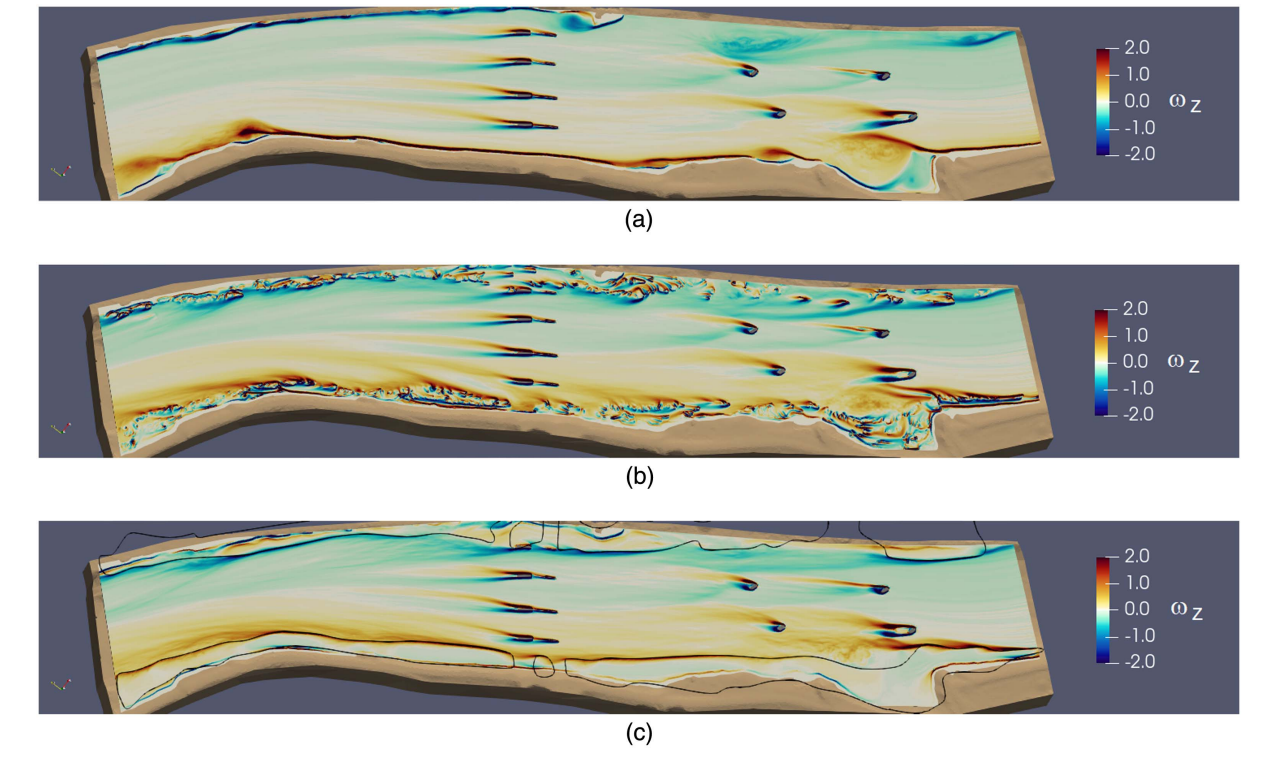


Fig. 12. Contours of time-averaged out-of-plane vorticity (ω_z) near water surface for (a) case with no vegetation; (b) case with resolved trees; and (c) case with vegetation model. The lines near the banks represent vegetated regions. The vorticity ω_z is normalized with the bulk velocity (U=2.4 m/s) and flow depth. The mean-flow depth is ~12.2 m and is conveyed from right to left.

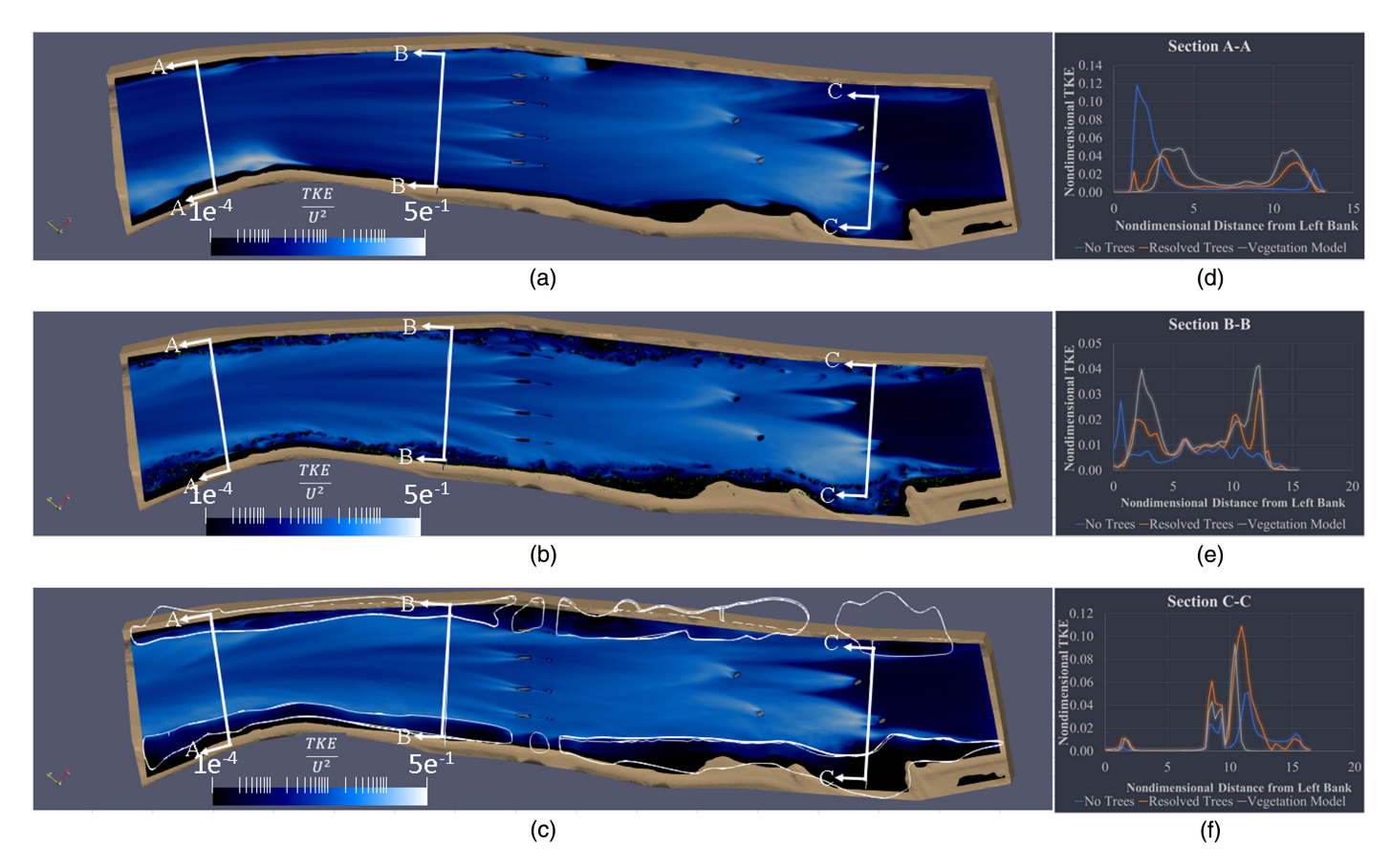


Fig. 13. Contours of TKE normalized by U^2 values for (a) case without trees; (b) case with resolved trees; and (c) case with vegetation model. The three lines across the river in each figure are the location of cross-sections indicating how the TKE compares for each case in which Sections A-A, B-B, and C-C are indicated in (d-f). The mean-flow depth is ~12.2 m and is conveyed from right to left.

Although the effect on the flow velocity distribution for both cases that incorporated trees is very similar, Fig. 12 indicates a difference in the number of vortices generated in the two cases. The vegetation model by design extracts momentum from the flow and dampens the vortex structures; whereas vortices are shed from these structures when the trees are resolved, thereby generating additional turbulent structures in the flow. However, Figs. 13(a-c) indicate the TKE for the case without trees, the tree-resolving case, and the vegetation model, respectively. These plots indicate that both vegetation approaches tend to reduce the TKE near the areas with trees and increase the TKE in the middle of the river. The relative difference in the TKE between each vegetation modeling approach is highlighted in Figs. 13(d and e). Within the trees or vegetated areas, the TKE is reduced (negative Δ TKE values); however, immediately adjacent to the areas with trees, there is a local increase in TKE due to the shear layer. Future investigations into the size, energy level, and impact on sediment transport processes are required to more fully assess the significance of the additional vortices generated in the tree-resolving simulation.

To assess the potential impact on sediment transport, the time-averaged shear stress, τ , on the channel bed is plotted in Fig. 14. As observed, the relative values for τ can be compared to assess the qualitative influence of tree modeling on the bed shear stress distributions of each test case. Consistent with the velocity distributions, the shear stresses are indicated to be substantially reduced in the near-bank region and noticeably elevated in the center of the channel because of the vegetation. In Figs. 14(a and b), the increase in shear stress in the middle of the channel is substantial, with values indicated in Sections A-A and B-B in the images at 40% to 50% higher for the vegetated cases than the case without

trees. Generally, the two cases incorporating vegetation compared similarly with respect to the change in bed shear stress; however, small differences in shear stress magnitudes are observed due to differences in the spatial distribution of the individual trees versus vegetated model regions and the value of C_d selected for the vegetation model. These differences are further highlighted in Figs. 15(a and b) and indicate that the inclusion of trees into the simulation increases the bed shear stress in the middle of the channel, typically from 2 to 3 N/m². Fig. 15(c) clearly indicates that higher shear stresses exist along the left bank in the case with the resolved trees compared with the vegetation model. Such a result is significant in this case study because it demonstrates that one would underestimate the shear stress acting on the bed by approximately 40%-70% by neglecting to include vegetation in the simulation. Qualitatively, both simulations that account for vegetation have similar effects on the bed shear stress throughout the channel; however, the magnitude and specific locations impacted by these effects differ, as indicated in Fig. 15(c). Regardless, this effect not only influences the channel's overall sediment transport capacity but also can dictate key morphological changes in the river, such as the degree to and rate at which the channel might erode its banks and form bars. This effect also influences other important issues, such as whether the flow can remove an armor layer in the center of the channel and the magnitude of scour at structures such as bridge piers.

Finally, to investigate the sensitivity of C_d in the vegetation model, two additional cases were simulated. The original C_d value of 0.74 was changed to 0.30 and 1.00, and the same grid resolution and flow parameters were studied. Plots indicating how the time-and depth-averaged velocities compared with one another are

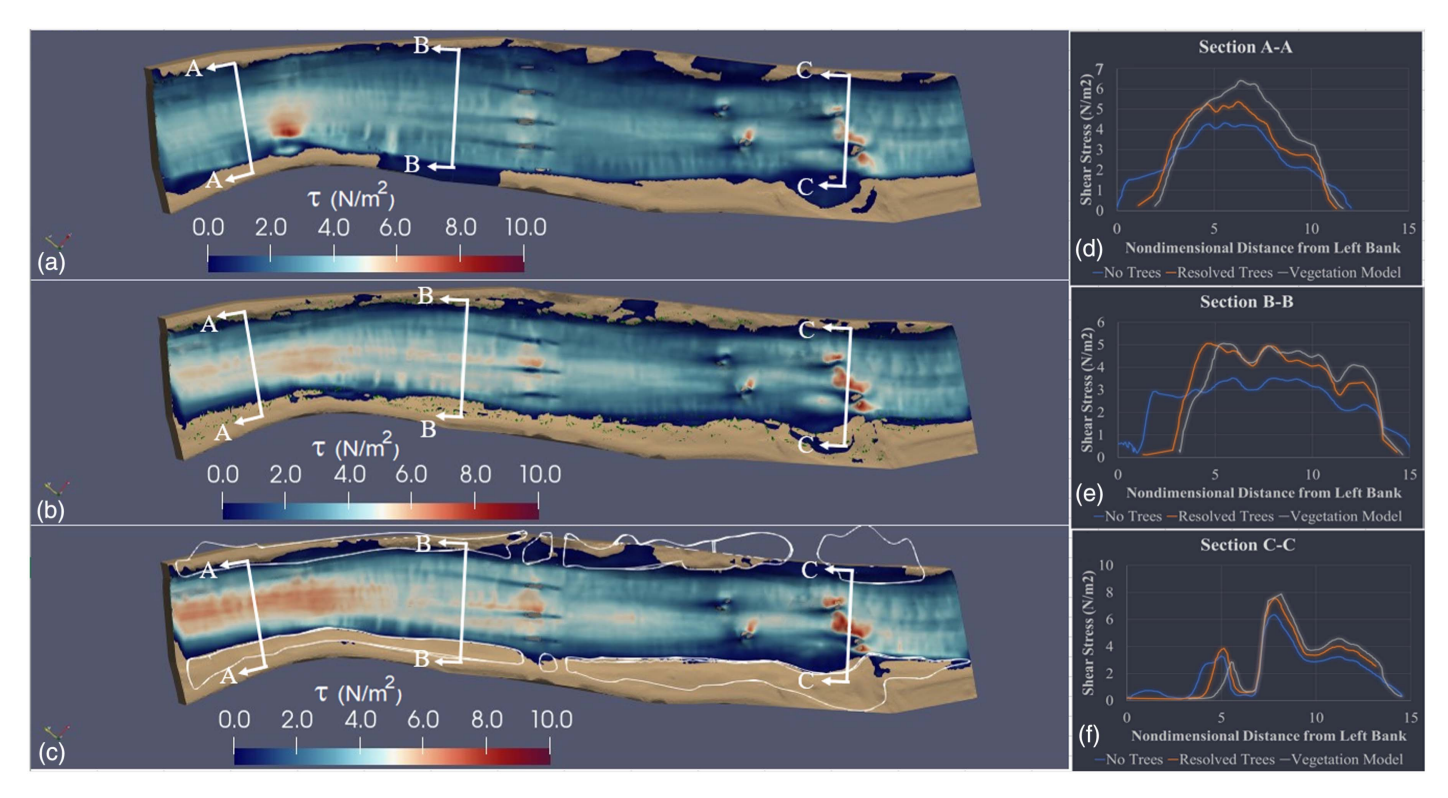


Fig. 14. Contours of time-averaged bed shear stress, τ , for (a) case without vegetation modeling; (b) case with resolved trees; and (c) case with vegetation model with vegetated regions outlined with the lines near the banks. The three lines across the river in each figure are the cross-section locations indicating how the bed shear stress compares for each case in which Sections A-A, B-B, and C-C are indicated in (d–f), respectively. Flow is from right to left.

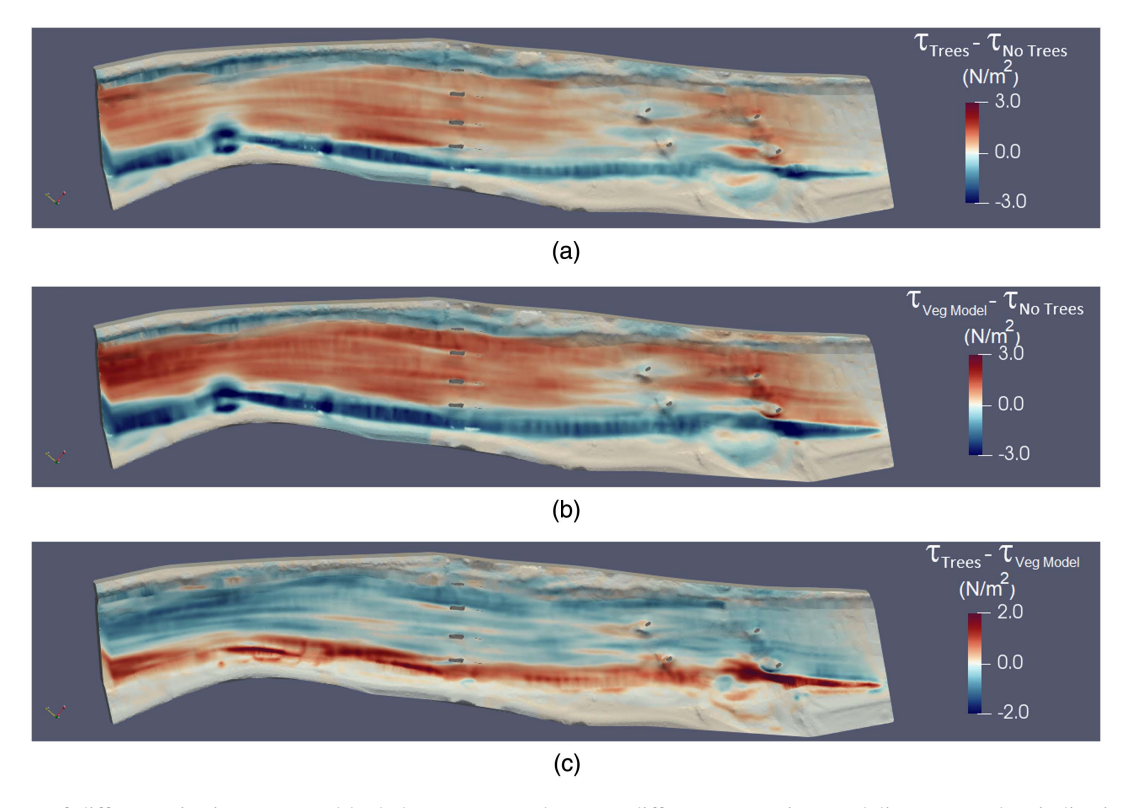


Fig. 15. Contours of difference in time-averaged bed shear stress, τ , between different vegetation modeling approaches indicating (a) difference between the tree-resolving approach and the case without trees; (b) difference between the case using the vegetation model and the case without trees; and (c) difference between the case with resolved trees and that with the vegetation model. Flow is from right to left.

indicated in Fig. S5. Counter to Yokojima et al. (2015), who concluded that the impact of C_d was not significant in the application of the vegetation model, our LES results indicate a small impact. For instance, when the drag coefficient along the bank is reduced from 0.74 to 0.30, the flow velocity in the vegetation region increases by approximately 0.2 m/s, in turn decreasing the velocity magnitude by approximately 0.1 m/s near the center of the river [Fig. S5(a)]. Increasing the value of C_d from 0.74 to 1.00 caused a similar redistribution of flow away from the banks [Fig. S5(b)]; however, the magnitude of this change is lower. This reduced impact can be attributed to most of the velocities near the bank already being minimal when C_d is 0.74.

Conclusions

Trees along the banks of natural rivers heavily influence the characteristics of flood flow in natural rivers. Incorporating vegetation into high-fidelity computational models is imperative for obtaining accurate modeling results. In this study, when trees were accounted for in large-eddy simulations, a drastic effect on redistributing the high-velocity flow away from the banks and increasing its magnitude near the center of the American River was observed. We demonstrated this effect using two separate modeling approaches: (1) resolving individual trees using the IBM; and (2) implementing a vegetation model to extract momentum in regions with trees. Both the tree-resolving approach and vegetation model similarly demonstrated a redistribution of flow effect. Generally, velocities in the center of the river increased by approximately 50% compared with the bulk velocity and were nearly damped out entirely along the banks. A second important effect of trees in models was their influence on the turbulence levels throughout the river.

Vortices are created along the shear layers adjacent to the banks and shed from the tree. Such effects were observed to be more prominent in the tree-resolving LES and the vegetation model. However, the tree resolving case indicated higher increases in turbulence compared with the vegetation model LES. This difference might become important in sediment transport and will be studied in detail in future studies. Moreover, comparing the bed shear stress levels in this study indicated that trees generally reduced stress within their immediate vicinity and appreciably increased shear stress on the bed in the center of the channel. Although it is recognized that the results from the study are necessarily site-specific to the case studied, these results can also provide researchers and engineers with an improved understanding of the importance and means of including vegetation into high-fidelity models to improve the accuracy of modeling predictions for flow and sediment processes in natural rivers.

Finally, the vegetation model requires the use of a drag coefficient, which is not well defined for trees in natural rivers. The value of this parameter indicated an appreciable impact on the time-averaged velocity results. Further investigation is required to calibrate and improve the confidence in the numerical modeling of riverine vegetation. Such studies could have significant implications for full-scale simulations of natural rivers for those interested in addressing bank erosion or meander migration, design of hydraulic structures or infrastructure, aquatic habitat or river restoration, to name a few. Additional studies with the vegetation model will be pursued to study the sensitivity of the model to the frontal area density function. Furthermore, field investigations to measure the flow velocities during high flows are planned to validate the full-scale influence of trees on the flow and sediment transport at this site.

Data Availability Statement

Some or all of the data, models, or code that support the findings of this study are available from the corresponding author on reasonable request. (LES flow field data, digital map of the study area, vegetation model, and VFS-Geophysics code.)

Acknowledgments

This work was supported by a grant from the National Science Foundation (EAR-0120914). The bathymetric survey data were supported by the California Department of Transportation. Computational resources were provided by the Center for Excellence in Wireless and Information Technology (CEWIT) of the College of Engineering and Applied Sciences at Stony Brook University.

Notation

The following symbols are used in this paper:

 A_f = projected area of vegetation;

 C_d = drag coefficient;

 F_i = canopy drag force;

g = gravitational acceleration;

 $H = \text{mean flow depth } \sim 12.2 \,\text{m};$

h = tree height;

P =fluid pressure;

t = time;

 $U = \text{mean-flow velocity} = 2.24 \,\text{m/s};$

u, v, and w = instantaneous velocity components;

V =time-averaged velocity magnitude;

 ρ = density of water;

 ν = kinematic viscosity of water; and

 ω_z = out of plane vorticity.

Supplemental Materials

Figs. S1–S5 are available online in the ASCE Library (www.ascelibrary.org).

References

- Calderer, A., X. Yang, D. Angelidis, A. Khosronejad, T. Le, S. Kang, A. Gilmanov, L. Ge, and I. Borazjani. 2015. Virtual flow simulator. Rep. No. VFS-Wind; 004806MLTPL00. Minneapolis: Univ. of Minnesota.
- Carollo, F. G., V. Ferro, and D. Termini. 2002. "Flow velocity measurements in vegetated channels." J. Hydraul. Eng. 128 (7): 664–673. https://doi.org/10.1061/(ASCE)0733-9429(2002)128:7(664).
- Choi, S. U., and H. Kang. 2004. "Reynolds stress modeling of vegetated open-channel flows." *J. Hydraul. Res.* 42 (1): 3–11. https://doi.org/10 .1080/00221686.2004.9641178.
- Constantinescu, G. 2014. "LES of shallow mixing interfaces: A review." Environ. Fluid Mech. 14 (5): 971–996. https://doi.org/10.1007/s10652 -013-9303-6.
- Constantinescu, G., M. Koken, and J. Zeng. 2011. "The structure of turbulent flow in an open channel bend of strong curvature with deformed bed: Insight provided by detached eddy simulation." Water Resour. Res. 47 (5): W05515. https://doi.org/10.1029/2010WR010114.
- Fischer-Antze, T., T. Stoesser, P. B. Bates, and N. R. Olsen. 2001. "3D numerical modelling of open-channel flow with submerged vegetation." *J. Hydraul. Res.* 39 (3): 303–310. https://doi.org/10.1080/00221680109499833.
- Garcia, M. H., F. Lopez, C. Dunn, and C. V. Alonso. 2004. "Flow, turbulence, and resistance in a flume with simulated vegetation." In *Riparian*

- vegetation and fluvial geomorphology, edited by S. J. Bennett and A. Simon, 11–27. Washington, DC: American Geophysical Union.
- Ge, L., and F. Sotiropoulos. 2007. "A numerical method for solving the 3D unsteady incompressible Navier-Stokes equations in curvilinear domains with complex immersed boundaries." *J. Comput. Phys.* 225 (2): 1782–1809. https://doi.org/10.1016/j.jcp.2007.02.017.
- Germano, M., U. Piomelli, P. Moin, and W. H. Cabot. 1991. "A dynamic subgrid-scale eddy viscosity model." *Phys. Fluids A* 3 (7): 1760–1765. https://doi.org/10.1063/1.857955.
- Ghisalberti, M., and H. M. Nepf. 2002. "Mixing layer and coherent structures in vegetated aquatic flows." J. Geophys. Res. 107 (C2): 11. https://doi.org/10.1029/2001JC000871.
- Gilmanov, A., and S. Acharya. 2008. "A hybrid immersed boundary and material point method for simulating 3D fluid-structure interaction problems." *Int. J. Numer. Methods Fluids* 56 (12): 2151–2177. https://doi.org/10.1002/fld.1578.
- Gilmanov, A., and F. Sotiropoulos. 2005. "A hybrid Cartesian/immersed boundary method for simulating flows with three-dimensional, geometrically complex, moving bodies." *J. Comput. Phys.* 207 (2): 457–492. https://doi.org/10.1016/j.jcp.2005.01.020.
- Gilmanov, A., F. Sotiropoulos, and E. Balaras. 2003. "A general reconstruction algorithm for simulating flows with complex 3D immersed boundaries on Cartesian grids." J. Comput. Phys. 191 (2): 660–669. https://doi.org/10 .1016/S0021-9991(03)00321-8.
- Jahra, F., Y. Kawahara, F. Hasegawa, and H. Yamamoto. 2011. "Flow-vegetation interaction in a compound open channel with emergent vegetation." *Int. J. River Basin Manage*. 9 (3–4): 247–256. https://doi.org/10.1080/15715124.2011.642379.
- Jeon, J., J. Y. Lee, and S. Kang. 2018. "Experimental investigation of three-dimensional flow structure and turbulent flow mechanisms around a nonsubmerged spur dike with a low length-to-depth ratio." Water Resour. Res. 54 (5): 3530. https://doi.org/10.1029/2017WR021582.
- Kang, S., C. Hill, and F. Sotiropoulos. 2016. "On the turbulent flow structure around an instream structure with realistic geometry." Water Resour. Res. 52 (10): 7869–7891. https://doi.org/10.1002/2016WR018688.
- Kang, S., A. Lightbody, C. Hill, and F. Sotiropoulos. 2011. "High-resolution numerical simulation of turbulence in natural waterways." Adv. Water Resour. 34 (1): 98–113. https://doi.org/10.1016/j.advwatres.2010 .09.018.
- Khosronejad, A., and K. Flora. 2018. "LES-and RANS-based modeling of coupled flow and mobile bed evolution in a natural river under various flood-induced turbulent boundary layers." In Vol. 63 of *Proc.*, *Bulletin* of the American Physical Society. College Park, MD: American Physical Society.
- Khosronejad, A., and K. Flora. 2019. "Three-phase flow LES of flash floods in a real-life desert stream." In *Proc., American Physics Society, Division of Fluid Dynamics Meeting Abstracts*. College Park, MD: American Physical Society.
- Khosronejad, A., K. Flora, and S. Kang. 2020a. "Effect of inlet turbulent boundary conditions on scour predictions of coupled LES and morphodynamics in a field-scale river: Bankfull flow conditions." *J. Hydraul. Eng.* 146 (4): 04020020. https://doi.org/10.1061/(ASCE)HY.1943 -7900.0001719.
- Khosronejad, A., K. Flora, Z. Zhang, and S. Kang. 2020b. "Large-eddy simulation of flash flood propagation and sediment transport in a dry-bed desert stream." *Int. J. Sediment Res.* 35 (6): 576–586. https://doi.org/10.1016/j.ijsrc.2020.02.002.
- Khosronejad, A., M. Ghazian Arabi, D. Angelidis, E. Bagherzadeha, K. Flora, and A. Farhadzadeh. 2019a. "Comparative hydrodynamic study of rigid-lid and level-set methods for LES of open-channel flow." J. Hydraul. Eng. 145 (1): 04018077. https://doi.org/10.1061/(ASCE) HY.1943-7900.0001546.
- Khosronejad, A., M. Ghazian Arabi, D. Angelidis, E. Bagherzadeha, K. Flora, and A. Farhadzadeh. 2020c. "A comparative study of rigid-lid and level-set methods for LES of open-channel flows: Morphodynamics." *Environ. Fluid Mech.* 20 (1): 145–164. https://doi.org/10.1007/s10652 -019-09703-y.
- Khosronejad, A., S. Kang, I. Borazjani, and F. Sotiropoulos. 2011. "Curvilinear immersed boundary method for simulating coupled flow and bed morphodynamic interactions due to sediment transport phenomena."

- Adv. Water Resour. 34 (7): 829–843. https://doi.org/10.1016/j.advwatres.2011.02.017.
- Khosronejad, A., S. Kang, A. Farhadzadeh, and F. Sotiropoulos. 2020d. "On the genesis and evolution of barchan dunes: Hydrodynamics." *Phys. Fluids* 32 (8): 086602. https://doi.org/10.1063/5.0015515.
- Khosronejad, A., S. Kang, and K. Flora. 2019b. "Fully coupled free-surface flow and sediment transport modelling of flash floods in a desert stream in the Mojave Desert, California." *Hydrol. Processes* 33 (21): 2772– 2791. https://doi.org/10.1002/hyp.13527.
- Khosronejad, A., S. Kang, and F. Sotiropoulos. 2012. "Experimental and computational investigation of local scour around bridge piers." Adv. Water Resour. 37 (Mar): 73–85. https://doi.org/10.1016/j.advwatres .2011.09.013.
- Khosronejad, A., L. Mendelson, A. Techet, S. Kang, A. Angelidis, and F. Sotiropoulos. 2020e. "Water exit dynamics of jumping archer fish: Integrating two-phase flow large-eddy simulation with experimental measurements." *Phys. Fluids* 32 (1): 011904. https://doi.org/10.1063/1 .5130886.
- Khosronejad, A., and F. Sotiropoulos. 2014. "Numerical simulation of sand waves in a turbulent open channel flow." J. Fluid Mech. 753 (2): 150–216. https://doi.org/10.1017/jfm.2014.335.
- Khosronejad, A., and F. Sotiropoulos. 2017. "On the genesis and evolution of barchan dunes: Morphodynamics." *J. Fluid Mech.* 815: 117–148. https://doi.org/10.1017/jfm.2016.880.
- Koken, M., and G. Constantinescu. 2008. "An investigation of the flow and scour mechanisms around isolated spur dikes in a shallow open channel: 1. Conditions corresponding to the initiation of the erosion and deposition process." Water Resour. Res. 44 (8): W08406. https://doi.org /10.1029/2007WR006489.
- Koken, M., G. Constantinescu, and K. Blanckaert. 2013. "Hydrodynamic processes, sediment erosion mechanisms, and Reynolds-number-induced scale effects in an open channel bend of strong curvature with flat bathymetry." J. Geophys. Res. 118 (4): 2308–2324. https://doi.org/10.1002/2013JF002760.
- Le, T., A. Khosronejad, F. Sotiropoulos, N. Bartelt, S. Woldeamlak, and P. DeWall. 2019. "Large-eddy simulation of the Mississippi River under base-flow conditions: Hydrodynamics of a natural diffluence-confluence region." J. Hydraul. Res. 57 (6): 836–851. https://doi.org/10.1080 /00221686.2018.1534282.
- Liu, C., and H. Nepf. 2016. "Sediment deposition within and around a finite patch of model vegetation over a range of channel velocity." Water Resour. Res. 52 (1): 600–612. https://doi.org/10.1002/2015WR018249.
- Liu, D., P. Diplas, J. D. Fairbanks, and C. C. Hodges. 2008. "An experimental study of flow through rigid vegetation." *J. Geophys. Res.* 113 (F4): F04015. https://doi.org/10.1029/2008JF001042.
- Lopez, F., and M. Garcia. 1996. "Turbulence and sediment transport in vegetated open channels: Simulation using two-equation turbulence models." In *Proc.*, 1st Int. Conf. on New Emerging Concepts for Rivers, 19–12. Paris: International Water Resources Association.

- Morinaga, T., N. Tanaka, J. Yagisawa, S. Karunaratne, and W. Weerakoon. 2012. Estimation of drag coefficient of trees considering the tree bending or overturning situations. Matala, Sri Lanka: Univ. of Ruhuna.
- Nepf, H. M. 1999. "Drag, turbulence, and diffusion in flow through emergent vegetation." Water Resour. Res. 35 (2): 479–489. https://doi.org/10.1029/1998WR900069.
- Patton, E. G. 1997. "Large-eddy simulation of turbulent flow above and within a plant canopy." Ph.D. thesis, Dept. of Land, Air, and Water Resources, UC Davis.
- Peters, R., E. Knudsen, G. Pauley, and J. Cederholm. 1996. Microhabitat selection by juvenile coho salmon in mainstem Clearwater River, 46. Olympia, Washington: US Fish and Wildlife Service, Wester Washington Fishery Resource Office.
- Poggi, D., A. Porporato, L. Ridolfi, J. D. Albertson, and G. G. Katul. 2004. "The effect of vegetation density on canopy sub-layer turbulence." *Boundary Layer Meteorol.* 111 (3): 565–587. https://doi.org/10.1023/B:BOUN.0000016576.05621.73.
- Shaw, R. H., and U. Schumann. 1992. "Large-eddy simulation of turbulent flow above and within a forest." *Boundary Layer Meteorol.* 61 (1): 47–64. https://doi.org/10.1007/BF02033994.
- Shimizu, Y., and T. Tsujimoto. 1993. "Comparison of flood-flow structure between compound channel and channel with vegetated zone." In *Proc.*, XXV IAHR Congress, 97–104. Madrid, Spain: International Association of Hydraulic Research.
- Smagorinsky, J. 1963. "General circulation experiments with the primitive equations. I: The basic experiment." Mon. Weather Rev. 91 (3): 99–164. https://doi.org/10.1175/1520-0493(1963)091<0099:GCEWTP>2.3.CO;2.
- Sonnenwald, F., V. Stovin, and I. Guymer. 2019. "Estimating drag coefficient for arrays of rigid cylinders representing emergent vegetation." J. Hydraul. Res. 57 (4): 591–597. https://doi.org/10.1080/00221686.2018.1494050.
- Stoesser, T., S. Kim, and P. Diplas. 2010. "Turbulent flow through idealized emergent vegetation." *J. Hydraul. Eng.* 136 (12): 1003–1017. https:// doi.org/10.1061/(ASCE)HY.1943-7900.0000153.
- Thorne, C. 1990. "Effects of vegetation on riverbank erosion and stability." In *Vegetation and erosion*, 125–144. New York: Wiley.
- Wilson, C., T. Stoesser, P. D. Bates, and A. Batemann Pinzen. 2003. "Open channel flow through different forms of submerged flexible vegetation." *J. Hydraul. Eng.* 129 (11): 847–853. https://doi.org/10.1061/(ASCE) 0733-9429(2003)129:11(847).
- Yokojima, S., Y. Kawahara, and T. Yamamoto. 2013. "Effect of vegetation configuration on turbulent flows in a rectangular open channel." In *Proc.*, 35th IAHR World Congress, A11875. Madrid, Spain: International Association of Hydraulic Research.
- Yokojima, S., Y. Kawahara, and T. Yamamoto. 2015. "Impacts of vegetation configuration on flow structure and resistance in a rectangular open channel." *J. Hydro-environ. Res.* 9 (2): 295–303. https://doi.org/10.1016/j.jher.2014.07.008.